even number of nodes so that it will interact mainly with d_{xz} (the z axis is perpendicular to the O_2N_2 plane and the x axis bisects the O–Fe–N angle). Hence d_{xz} must be placed in the MO diagram for the dimer (Figure 1b) such that it has a higher spin population in the $S' = 2$ state. Although an approximate MO diagram for some bent μ-oxo dimers has been proposed,[20] the low symmetry of the system and the lack of information concerning the exact ordering of the levels in the monomers renders any detailed analysis unrealistic at this stage. It is emphasized that none of the results obtained in this work imply that an MO description is to be preferred to the HDVV treatment of the electronic properties of the antiferromagnetic dimers. Studies of the related μ-oxo Fe(III) dimers derived from HEDTA[35,63,64] and EDTA[64] indicate that their magnetic and spectral properties can be adequately interpreted on the basis of high-spin ferric ions coupled by spin–spin interactions, with the separation of the $S' = 0, 1, 2$ states in accord with the predictions of the HDVV model.[63]

(63) M. Okamura, personal communication to G. N. L.
(64) H. J. Schugar, G. R. Rossman, C. G. Barraclough, and H. B. Gray, *J. Amer. Chem. Soc.*, **94**, 2683 (1972).

Lastly, it has been suggested that pmr spectra of oxo-bridged dimers in solution are well-resolved because magnetic exchange coupling decreases the electron spin relaxation time in the dimer relative to that in a related high-spin monomer. Although such coupling can lead to considerable decreases in T_{1e} for the metal center in some cases, T_{1e} for salen dimers is actually longer than for the monomers. In the fast motion limit the line width is given[52] by $\delta \propto \mu_e^2 T_{1e}$. Taking $\mu_e \approx 6$ BM for the monomer and ~ 2 BM for the dimer and using the experimental 4-H line widths in Table II, T_{1e} (monomer) $\sim 0.7 T_{1e}$ (dimer). Hence, relaxation in the monomer is more efficient, and the narrower lines in the dimer arise primarily from the appreciable population of the diamagnetic ground state. The improved resolution of the monomer spectrum compared to that of the dimer is evident in Figure 3.

Acknowledgment. The research at Massachusetts Institute of Technology was supported by Grants GM-15471 (National Institutes of Health) and GP-18978X (National Science Foundation). We thank Drs. A. Adler and D. Dolphin for supplying several of the compounds used in this study.

Stereochemically Nonrigid Six-Coordinate Molecules.[1] III. The Temperature-Dependent ^1H and ^{31}P Nuclear Magnetic Resonance Spectra of Some Iron and Ruthenium Dihydrides

P. Meakin, E. L. Muetterties, and J. P. Jesson*

Contribution No. 1947 from the Central Research Department, E. I. du Pont de Nemours and Company, Experimental Station, Wilmington, Delaware 19898. *Received June 20, 1972*

Abstract: Stereochemical nonrigidity in a class of six-coordinate hydrides has been examined using ^1H and ^{31}P nmr techniques. These hydrides are of the type H_2ML_4, where M is iron or ruthenium and L is a phosphite, phosphine, phosphinite, or phosphonite. The stereochemical behavior in solution for these complexes is of two types: (1) the cis stereoisomer with essentially no trans form present and (2) cis and trans forms present in equilibrium and both detectable by nmr. The rearrangement barriers for the iron complexes proved relatively insensitive to wide variations in the steric and electronic character of the phosphorus ligands. This situation also prevailed in the ruthenium set, but ruthenium barriers were larger than those for iron. The intramolecular rearrangements are discussed in terms of the "tetrahedral jump" model with consideration of the range of potential energy surfaces available for these fluxional molecules. A similar study was also carried out for complexes of the form H_2ML_3L' ($L' = CO, C_6H_5CN$).

Stereochemical nonrigidity is an established, common feature of five-, seven-, eight-, and nine-coordinate molecules or ions.[2-5] This is a primary reflection of the nondominance of any idealized coordination polyhedron in these coordination classes and the close physical relationships among the plausible, idealized coordination polyhedra within a class.[2-5] In contrast, six-coordinate molecules are much less prone to facile intramolecular rearrangement.[2-6] For this coordination number there is one predominant coordination polyhedron, the octahedron.[4,6] Recently we showed that a group of transition metal hydrides, of the type H_2ML_4, are stereochemically nonrigid.[7-9] This was the first[10] unequivocal demon-

(1) Paper II in this series: D. H. Gerlach, W. G. Peet, and E. L. Muetterties, *J. Amer. Chem. Soc.*, **94**, 4545 (1972).
(2) E. L. Muetterties, *Inorg. Chem.*, **4**, 769 (1965).
(3) E. L. Muetterties, *Accounts Chem. Res.*, **3**, 266 (1970).
(4) E. L. Muetterties, *Rec. Chem. Progr.*, **31**, 51 (1970).
(5) J. P. Jesson, P. Meakin, and E. L. Muetterties, *J. Amer. Chem. Soc.*, 93, 5261 (1971).
(6) E. L. Muetterties, *ibid.*, **90**, 5097 (1968).
(7) F. N. Tebbe, P. Meakin, J. P. Jesson, and E. L. Muetterties, *ibid.*, **92**, 1068 (1970).
(8) P. Meakin, L. J. Guggenberger, J. P. Jesson, D. H. Gerlach, F. N. Tebbe, W. G. Peet, and E. L. Muetterties, *ibid.*, 92, 3482 (1970).

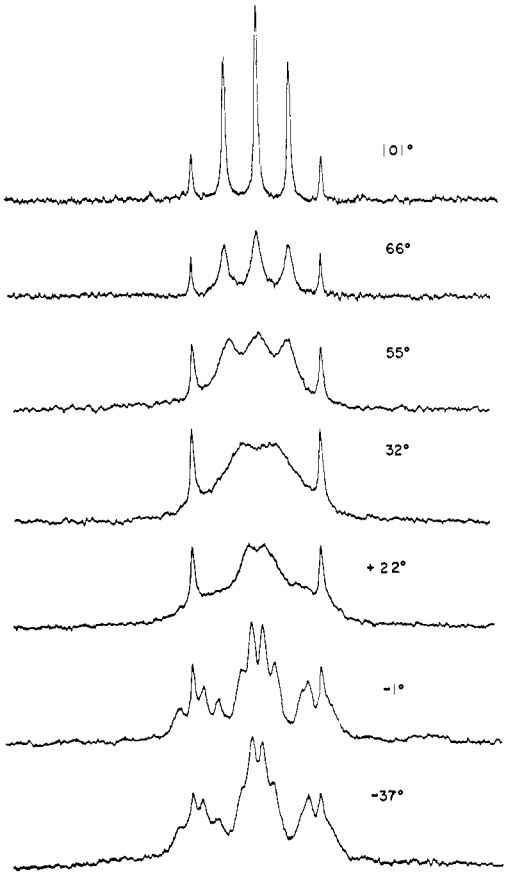

Figure 1. The temperature-dependent 220-MHz hydride region ^1H nmr spectrum of $H_2Fe[P(OCH_2)_3CC_2H_5]_4$ in toluene.

stration of fluxional behavior in six-coordinate molecules. Accordingly, we felt it important to try to define the steric and electronic facets that distinguish this group of hydrides from the majority of six-coordinate complexes. Our detailed study[9] of *cis*-$FeH_2[P(OC_2H_5)_3]_4$, from which both mechanistic and rate information was derived, suggested that the rearrangements could be rationalized in terms of a novel coordination polyhedron, a *pseudotetrahedron*, and that the picture would apply to many hydrides of the form H_xML_4. The concept is most easily seen in five-coordination ($x = 1$)[12] where in the ground state the P_4 framework can, in some cases, approach very closely a regular tetrahedron[13] with the hydrogen at the center of one of the faces. In the rearrangement process, the hydrogen may move from a face position to an edge with a concomitant increase in the PMP interbond angle (the transition state or intermediate) and then to a previously unoccupied face position. For H_2ML_4 systems similar considerations apply, but here the MP_4 substructure departs substantially from a regular tetrahedron as shown by X-ray studies.[14a] Cis and trans stereoisomers are of course possible in the H_2ML_4 molecules, and intrinsically the six-coordinate case is richer in mechanistic information.

There are subtle features in the rearrangement mechanism for the H_2ML_4 molecules. For example, the nmr studies[9] could not distinguish between a *concerted motion* in which a single hydrogen atom changed facial positions and a two-step process involving a *reaction intermediate* with hydrogen nuclei at trans edges of a nearly regular tetrahedron. These two alternative rearrangement mechanisms and the qualitative features of the structural and dynamic characteristics of the H_2ML_4 hydrides are examined in detail in this paper. Full discussion of other X-ray structural studies will be presented shortly.[14b]

A. Experimental Section

The preparation of the iron and ruthenium dihydrides studied in this work is described elsewhere.[1]

Nmr samples were prepared in a nitrogen atmosphere (Vacuum Atmospheres Dri Lab; less than 2 ppm of O_2) using deoxygenated solvents. Unless otherwise stated, toluene or toluene-d_8 was the solvent. Variable-temperature proton nmr spectra were recorded using a Bruker HFX-90 and Varian HR-220 and HA-100 spectrometers. The ^{31}P spectra (36.43 MHz) were measured with and without proton noise decoupling using the Bruker spectrometer. The ^{31}P samples were run in 10-mm tubes with 3-mm coaxial capillaries containing hexafluorobenzene or 1,2-dibromotetrafluoroethane (depending on the temperature) for field-frequency stabilization. Temperatures for the spectra taken on the HR-220 were measured either by observing the chemical shift separation in methanol or ethylene glycol samples run before and after each trace or by means of a thermometer which fits inside the spinning nmr tube. For the HFX-90, temperatures were measured by means of a copper–constantan thermocouple located just beneath the sample tube and were calibrated using a similar thermocouple held coaxially in the spinning sample tube partially filled with solvent. The temperature controller on the HA-100 was calibrated using methanol or ethylene glycol depending on the temperature.

Nmr line shapes in the presence of exchange were simulated using the density matrix method of Kaplan[15] and Alexander.[16] The details of these calculations are described elsewhere.[9] The exchange rates were determined by varying the rates used in the calculations until a best visual fit was obtained between the calculated and observed spectra.

B. Stereochemistry of the H_2ML_4 Complexes in Solution

(1) The Iron Dihydrides. The stereochemistry of the iron dihydrides in solution can be established on the basis of the low-temperature limit ^1H and ^{31}P nmr spectra. The slow-exchange-limit hydride region proton nmr spectra at 220 MHz for most dihydrides consist of a complex, nearly symmetric pattern that can be crudely described as a doublet of triplets[7-9] or a quartet of triplets (Figure 1). Such a pattern is diagnostic of cis stereochemistry (Figure 2) with the dominant triplet structure arising from the coupling of the hydride protons to the two magnetically equivalent phosphorus nuclei P_1 and P_2 (the labeling scheme for the nuclei is shown in Figure 2). At lower fields (60, 90, and 100 MHz), the spectra are generally asymmetric[9] because

(9) P. Meakin, E. L. Muetterties, F. N. Tebbe, and J. P. Jesson, *J. Amer. Chem. Soc.*, 93, 4701 (1971) (part I of this series).

(10) Since our initial reports, a series of papers has appeared that strongly implicate stereochemical nonrigidity in certain six-coordination chelates; *cf.* ref 11 and leading references therein. Also, R. K. Pomeroy and W. A. Graham (*ibid.*, 94, 274 (1972)) have described fluxional $M(CO)_4(SiR_3)_2$ molecules.

(11) (a) L. H. Pignolet, R. A. Lewis, and R. H. Holm, *ibid.*, 93, 360 (1971); (b) *Inorg. Chem.*, 11, 99 (1972); (c) S. S. Eaton, J. R. Hutchison, R. H. Holm, and E. L. Muetterties, *J. Amer.Chem. Soc.*, 94, 6411 (1972).

(12) P. Meakin, E. L. Muetterties, and J. P. Jesson, *ibid.*, 94, 5271 (1972).

(13) B. A. Frenz and J. A. Ibers in "Transition Metal Hydrides," E. L. Muetterties, Ed., Marcel Dekker, New York, N. Y., 1971, Chapter 3.

(14) (a) L. J. Guggenberger, D. D. Titus, M. T. Flood, R. E. Marsh, A. A. Orio, and H. B. Gray, *J. Amer. Chem. Soc.*, 94, 1135 (1972); (b) L. J. Guggenberger, to be submitted for publication.

(15) J. I. Kaplan, *J. Chem. Phys.*, 28, 278 (1958); 29, 462 (1958).

(16) S. Alexander, *ibid.*, 37, 967, 974 (1962); 38, 1787 (1962); 40, 2741 (1964).

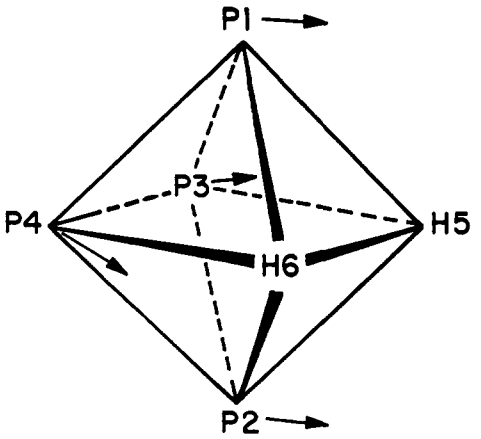

Figure 2. Nuclear labeling scheme and departure from idealized octahedral geometry for *cis*-H_2ML_4 complexes. Arrows indicate the direction of displacement of the phosphorus nuclei.

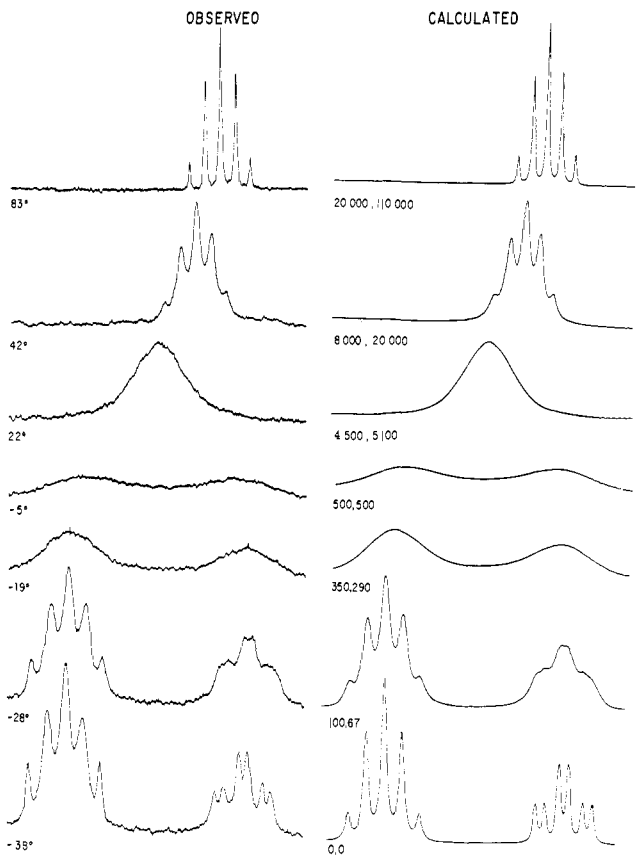

Figure 3. The temperature-dependent 220-MHz hydride region ^1H nmr spectrum of $H_2Fe[PC_6H_5(OCH_3)_2]_4$ in toluene with corresponding spectra simulated using a first-order approximation and a random exchange permutational mechanism. The numbers under the simulated spectra indicate the cis → trans and trans → cis exchange rates, respectively. The equilibrium constant K_{eq}(cis/trans) is given by rate (trans → cis)/rate (cis → trans). The low-field end of the spectrum is at the left side.

the ^{31}P chemical shift separations are then comparable to the P–P coupling constants. In several cases the cis structure has been confirmed by the proton noise decoupled ^{31}P spectra which are A_2B_2 patterns.[7,9] Nmr parameters for the proton noise decoupled ^{31}P spectra are listed in Table I. The 220-MHz hydride region ^1H nmr spectra of $H_2Fe[(CH_3)_2PCH_2CH_2P(CH_3)_2]_2$ and $H_2Fe[(C_6H_5)_2PCH_2CH_2P(C_6H_5)_2]_2$ have a

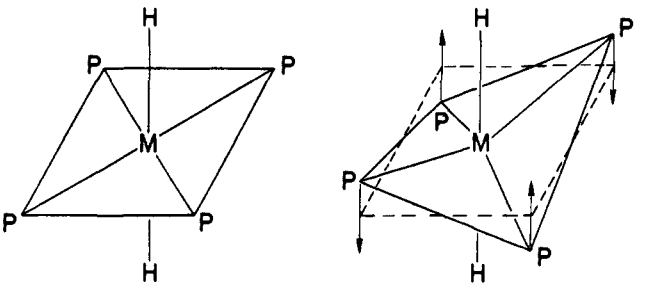

Figure 4. D_{4h} and D_{2d} structures for the *trans*-H_2ML_4 dihydrides in solution. The inversion mode is shown for the S_4 geometry.

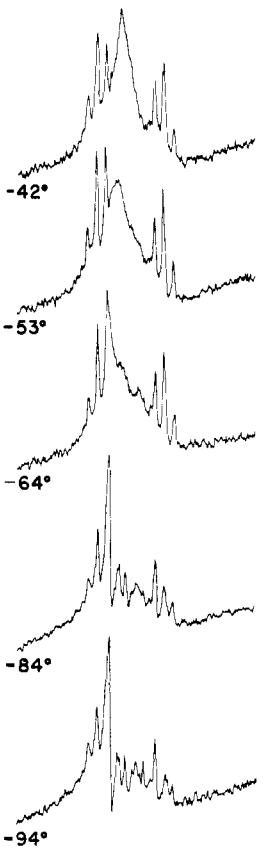

Figure 5. Proton noise decoupled ^{31}P (36.43 MHz) nmr spectrum for $H_2Fe[PC_6H_5(OCH_3)_2]_4$ in toluene over a range of low temperatures. Above −42° the spectrum broadens and then coalesces into a sharp single line at about 50°.

Table I. ^{31}P Nmr Parameters for Some Iron Dihydrides at the Low-Temperature Limit in Toluene[a]

Compound	$\|J\|$[b]	δ[c]	Average shift[d]
$H_2Fe[P(CH_3)_2C_6H_5]_4$	24	1.07	−35.0
$H_2Fe[(CH_3)_2PCH_2CH_2P(CH_3)_2]_2$[e]	26	9.74	−66.7
$H_2Fe[P(C_6H_5)_2CH_3]_4$	15	5.90	−51.5
$H_2Fe\{o\text{-}C_6H_4[P(C_2H_3)_2]_2\}_2$			−108.6 (trans)
$H_2Fe[P(OC_6H_5)_3]_4$	62	5.65	−158.9
$H_2Fe[P(OCH_2)_3CC_2H_5]_4$	58	3.27	−160.2
$H_2Fe[P(OC_2H_5)_3]_4$	56	2.20	−184.2
$H_2Fe[P(OC_2H_5)_2C_6H_5]_4$	45	10.87	−193.3 (cis)
			−193.5 (trans)
$H_2Fe[P(OCH_3)_2C_6H_5]_4$	46	8.98	−198.7 (cis)
			−199.6 (trans)

[a] Taken from the A_2B_2 proton noise decoupled ^{31}P spectra. [b] $J_{13} = J_{14} = J_{23} = J_{24}$ coupling constants in Hz. [c] Chemical shift differences for the two ^{31}P environments (ppm). [d] Ppm upfield from 85% H_3PO_4. [e] AA'BB' spectrum not distinguishable from A_2B_2 in this case.

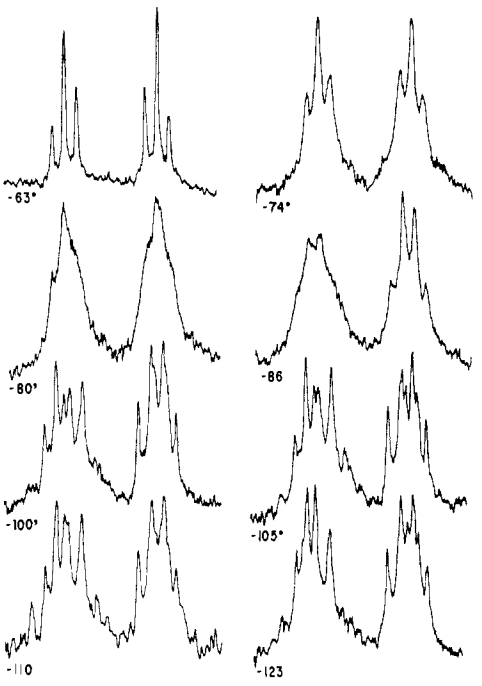

Figure 6. Temperature-dependent proton noise decoupled ^{31}P nmr spectra of $H_2Fe[PC_6H_5(OCH_3)_2]_4$ taken at 36.43 MHz in 50% CH_2Cl_2–50% CHF_2Cl. In this solvent the cis–trans equilibrium strongly favors the cis isomer.

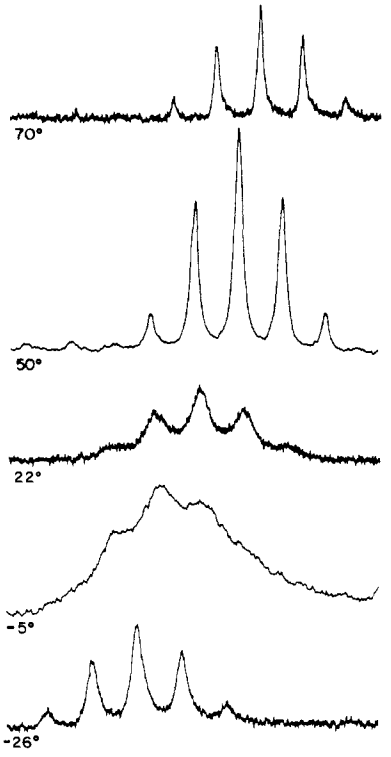

Figure 7. The temperature-dependent 220-MHz hydride region ^1H nmr spectra of $H_2Fe\{o\text{-}C_6H_4[P(C_2H_5)_2]_2\}_2$ in toluene. The low-field end of the spectrum is at the left side.

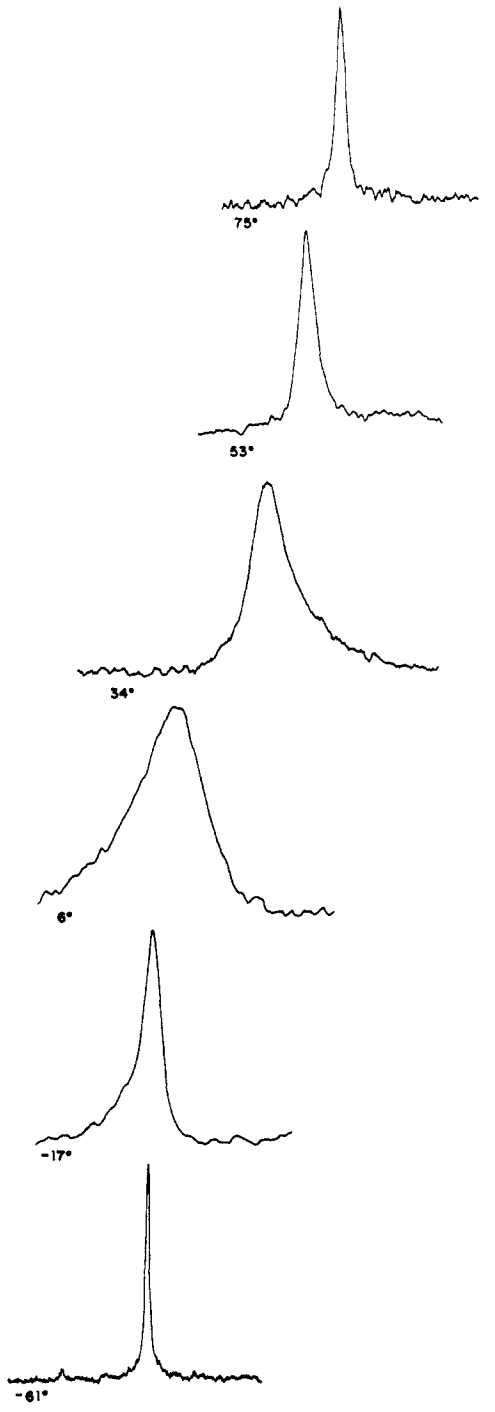

Figure 8. The temperature-dependent ^1H noise decoupled ^{31}P (36.43 MHz) nmr spectrum associated with $H_2Fe\{o\text{-}C_6H_4[P(C_2H_5)_2]_2\}_2$ in toluene.

more complex appearance than those associated with the *cis*-iron dihydrides with unidentate ligands and have not been analyzed in detail. These spectra are, however, too complex to arise from a trans molecule and are assigned to a cis structure, consistent with the observation of AA′BB′ patterns in the proton noise decoupled ^{31}P spectra.

Of the 16 iron dihydrides investigated, 13 have exclusively cis stereochemistry in solution. In two cases, $H_2Fe[PC_6H_5(OC_2H_5)_2]_4$ and $H_2Fe[PC_6H_5(OCH_3)_2]_4$, the high-field proton nmr spectra at −50° consist of a doublet of triplets, assigned to the cis isomer, and a quintet, assigned to the trans isomer (Figure 3). A D_{4h} structure (Figure 4) for the trans isomer should have a hydride ^1H nmr spectrum consisting of a binomial quintet while the less symmetric D_{2d} structure (Figure 4) could yield a complex, symmetric spectrum

Table II. Hydride Region ^1H Nmr Parameters for Some Iron Dihydrides in Toluene

Complex	ΣJ_{HP}[a] (temp, °C)	δ[b] (temp, °C)
$H_2Fe[P(OCH_2)_3CC_2H_5]_4$	131 (28)	12.0 (28)
$H_2Fe[P(OC_2H_5)_3]_4$	151.5 (28)	13.9 (28)
$H_2Fe[P(O\text{-}i\text{-}C_3H_7)_3]_4$	168 (28)	14.4 (28)
$H_2Fe[P(OC_6H_5)_3]_4$	147 (22)	12.2 (22)
$H_2Fe[P(O\text{-}o\text{-}C_7H_7)_3]_4$	168 (35)	11.9 (35)
$H_2Fe[P(C_6H_5)(OCH_3)_2]_4$	194 (trans), 153 (cis) (−45)	10.5 (trans), 12.7 (cis) (−45)
$H_2Fe[P(C_6H_5)(OC_2H_5)_2]_4$	195 (trans), 157 (cis) (−50)	10.6 (trans), 13.0 (cis) (−50)
$H_2Fe[(C_6H_5)(O\text{-}i\text{-}C_3H_7)_2]_4$	154 (21)	14.0 (21)
$H_2Fe[P(C_6H_5)(CH_3)_2]_4$	173 (22)	14.2 (22)
$H_2Fe[P(C_6H_5)(C_2H_5)_2]_4$	188 (22)	15.8 (22)
$H_2Fe[P(C_6H_5)_2(CH_3)]_4$	178 (28)	13.8 (28)
$H_2Fe[P(CH_3)_3]_4$	170 (10)[c]	13.3 (10)[c]
$H_2Fe[PF_3]_4$		12.2 (28)
$H_2Fe[(C_6H_5)_2PCH_2CH_2P(C_6H_5)_2]_2$	139 (22)	16.4 (22)[d]
$H_2Fe[(CH_3)_2PCH_2CH_2P(CH_3)_2]_2$	135 (80)	14.1 (22)
$H_2Fe\{o\text{-}C_6H_4[P(C_2H_5)_2]_2\}_2$	166 (−26)	12.8 (−26)
$H_2Fe[P(C_6H_5)_2(CH_3)]_3CO$		9.5, 11.6 (−30)
$H_2Fe[P(C_6H_5)_2(C_2H_5)]_3CO$		9.6; 11.7 (−32)

[a] $|(J_{15} + J_{25} + J_{35} + J_{45})|$ in Hz. [b] Ppm upfield from TMS. [c] H. F. Klein, *Angew. Chem., Int. Ed. Engl.*, **9**, 904 (1970). [d] From glyme in $(C_6H_5)_2O$.

consisting of many transitions with the spectral envelope resembling a nonbinomial symmetric quintet. The latter alternative was observed for *trans*-$H_2Fe[PC_6H_5(OC_2H_5)_2]_4$ and *trans*-$H_2Fe[PC_6H_5(OCH_3)_2]_4$. In each case, the outer two lines of the quintet appear to be narrower than the remaining lines (Figure 3), and it is clear that the equilibrium structures have less than D_{4h} symmetry.

The ^1H noise decoupled ^{31}P spectrum corresponding to either the D_{4h} or D_{2d} structures should be a sharp singlet. However, for both $H_2Fe[PC_6H_5(OCH_3)_2]_4$ and $H_2Fe[PC_6H_5(OC_2H_5)_2]_4$ the noise decoupled ^{31}P spectrum at −50° consists of an A_2B_2 pattern assigned to the cis structure together with a very broad resonance (Figure 5). On further cooling the broad resonance sharpens into a complex spectrum containing an intense single line which may be the singlet spectrum of the trans isomer. The remainder of the low-temperature-limit spectrum is complex and asymmetric, indicating a species of low symmetry. It is attractive to speculate that this species may correspond to an additional isomer of the dihydrides in which the two hydrogens are located in the face and edge positions, respectively, of an approximately regular tetrahedral disposition of the four ligand phosphorus atoms. Such a structure could correspond to an intermediate in the cis ↔ cis "tetrahedral jump" exchange process and also in the cis ↔ trans exchange process. However, an alternative and perhaps more plausible interpretation of these spectra is that the bulky ligands interact in such a way as to reduce the symmetry of the trans molecule below that shown in Figure 4 (D_{4h} or D_{2d}) and that the ligand motions are sufficiently restricted that the reduction of symmetry is maintained on the nmr time scale. The nonbinomial quintet hydride region proton nmr spectra for the isomers in the temperature range −65 to −30° may be interpreted as either of the following.

(a) The high-temperature region of an exchanging system in which the high-temperature-limit nmr Hamiltonian has D_{2h} symmetry. The variation of the line widths in the quintet can in this case be attributed to the high-temperature limit having not been reached.

(b) The high-temperature region of an exchanging system in which the averaged nmr Hamiltonian has D_{2d} symmetry as shown in Figure 4. In this case the nonbinomial quintet may represent the high-temperature-limit spectrum.

A similar reduction of symmetry is observed in the cis isomers. On cooling below about −70°, the A_2B_2 proton noise decoupled ^{31}P nmr spectra of *cis*-$H_2Fe[PC_6H_5(OC_2H_5)_2]_4$ and *cis*-$H_2Fe[PC_6H_5(OCH_3)_2]_4$ first broaden and then sharpen into a complex pattern consistent with a ^{31}P spin system of low symmetry and/or a complex mixture of isomers (Figure 6). We have previously suggested[8] that the broadening of the hydride region ^1H nmr spectra of $H_2Fe\{PC_6H_5[OCH(CH_3)_2]_2\}_4$ at low temperatures may be due to restricted motions in the ligands. In the solid phase, the structure[8,14] of $H_2Fe[PC_6H_5(OC_2H_5)_2]_4$ differs appreciably from the idealized C_{2v} symmetry shown in Figure 2; this distortion is probably due more to interligand interactions rather than crystal packing effects.

For $H_2Fe\{o\text{-}C_6H_4[P(C_2H_5)_2]_2\}_2$ (**1**), the low-temperature-limit hydride region ^1H nmr spectrum consists of a near binomial quintet (Figure 7), and the noise decoupled ^{31}P spectrum is a sharp singlet in the same temperature range (Figure 8). These observations require a trans structure in the low-temperature limit in agreement with the results of Chatt, *et al.*,[17] for this molecule. There is no detectable signal in either the ^1H or ^{31}P nmr spectra for the cis isomer at low temperatures, but line shape changes show that the cis isomer is present and is present in high concentrations at elevated temperatures (*vide infra*).

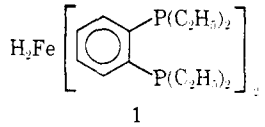

1

^1H chemical shift data for the iron dihydrides are given in Table II. The hydride chemical shifts are essentially temperature independent (for both the cis and trans isomers). For example, in $H_2Fe[P(OC_2H_5)_3]_4$

(17) J. Chatt, F. A. Hart, and R. G. Hayter, *Nature (London)*, **187**, 55 (1960); J. Chatt and R. G. Hayter, *J. Chem. Soc.*, 2605, 5507 (1961); J. Chatt, F. A. Hart, and D. T. Rosevear, *ibid.*, 5504 (1961).

Table III. Hydride Region ^1H Nmr Parameters for Some H_2RuL_4 Complexes in Toluene-d_8

Compound	ΣJ_{HP}[a]	Shift[b]
$H_2Ru[P(OCH_3)_3]_4$	31	10.2
$H_2Ru[P(OC_2H_5)_3]_4$	30	10.3
$H_2Ru[P(O\text{-}i\text{-}C_3H_7)_3]_4$	30	10.5
$H_2Ru[P(C_6H_5)(OCH_3)_2]_4$	84 (trans), 16 (cis)	6.6 (trans), 9.3 (cis)
$H_2Ru[P(C_6H_5)(OC_2H_5)_2]_4$	85 (trans), 14 (cis)	6.1 (trans), 9.3 (cis)
$H_2Ru[P(C_6H_5)(O\text{-}i\text{-}C_3H_7)_2]_4$	84 (trans), 19 (cis)	5.7 (trans), 10.3 (cis)
$H_2Ru[P(C_6H_5)_2(OCH_3)]_4$	2	9.0
$H_2Ru[P(C_6H_5)(CH_3)_2]_4$	9	9.5
$H_2Ru[P(C_6H_5)(C_2H_5)_2]_4$	18	11.1
$H_2Ru[P(C_6H_5)_2(CH_3)]_4$	9	9.4
$H_2Ru[PF_3]_4$		8.9
$H_2Ru[(C_6H_5)_2PCH_2CH_2P(C_6H_5)_2]_2$	5	8.4
$H_2Ru[P(C_6H_5)_2(CH_3)]_3CO$		6.6, 8.0
$H_2Ru[P(C_6H_5)_3]_3C_6H_5CN$		13.8, 8.6
$H_2Ru[PC_6H_5(C_2H_5)_2]_3CO$		6.7, 8.1

[a] Separation of sharp inner lines = $|(J_{15} + J_{25} + J_{35} + J_{45})|$. [b] Ppm upfield from TMS.

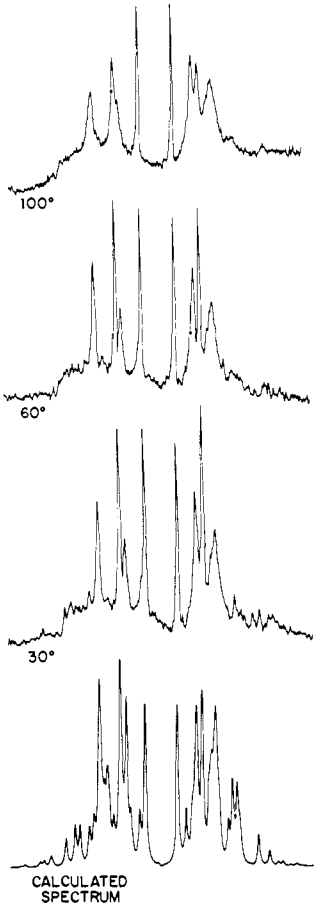

Figure 9. Observed and calculated 90-MHz hydride region ^1H nmr spectra for $H_2Ru[P(OCH_3)_3]_4$. The low-field end of the spectrum is at the right side. The simulated slow-exchange-limit spectrum is shown on the bottom row.

(toluene-d_8), the temperature dependence of the chemical shift is only 1×10^{-3} ppm deg^{-1} over the temperature range -50 to $+80°$. In addition the values for the sum of the H–P coupling constants (equal to the separation of the sharp outer lines which are invariant to the exchange process[7-9]) are given in Table II; again the parameter is nearly temperature independent ($\sim$0.025 Hz deg^{-1} for $H_2Fe[P(OC_2H_5)_3]_4$ over the temperature range 0–80°).

(2) The Ruthenium Dihydrides. The low-temperature-limit (room temperature) hydride ^1H nmr spectra of nine of the 12 ruthenium dihydrides which were investigated can be interpreted exclusively in terms of a cis stereochemistry.[8,18] Figure 9 compares the observed hydride spectra of $H_2Ru[P(OCH_3)_3]_4$ with a spectrum simulated, assuming a cis structure (Figure 2) using the following nmr parameters: J_{12} unknown – magnetic equivalence, $J_{13} = J_{23} = J_{14} = J_{24} = 41$ Hz, $J_{15} = J_{16} = J_{25} = J_{26} = -24$ Hz, $J_{34} = -4$ Hz, $J_{35} = J_{46} = -20$ Hz, $J_{36} = J_{45} = 99$ Hz, $J_{56} = -14$ Hz, δ_{56} 10.2 ppm upfield from TMS, $\delta_{34} - \delta_{12} = 3.4$ ppm (-124 Hz at 36.43 MHz), $(\delta_{34} + \delta_{12})/2 = 171.9$ ppm upfield from 85% H_3PO_4.

At 220 MHz the hydride region ^1H nmr spectra of most, but not all (see Figure 9), of the *cis*-ruthenium dihydrides have the appearance of a sharp doublet of triplets superimposed on a broad background.[8,18] The triplet splitting is again due to coupling of the hydride protons to the two magnetically equivalent ^{31}P nuclei, P_1 and P_2, as in the case of the iron dihydrides. However, the doublet separation is equal to the sum of the coupling constant beween a hydride proton and the ^{31}P nuclei, P_3 and P_4 (*e.g.*, $J_{53} + J_{54}$) and unlike the iron dihydrides is of opposite sign and greater magnitude than the triplet separation ($J_{15} = J_{25}$ = etc.). The $|H(\alpha\alpha); P(\alpha\alpha\alpha\alpha)\rangle \rightarrow |H(\alpha\beta + \beta\alpha); P(\alpha\alpha\alpha\alpha)\rangle$ and $|H(\alpha\beta + \beta\alpha); P(\alpha\alpha\alpha\alpha)\rangle \rightarrow |H(\beta\beta); P(\alpha\alpha\alpha\alpha)\rangle$ transitions and the corresponding transitions with $P(\beta\beta\beta\beta)$ in place of $P(\alpha\alpha\alpha\alpha)$ which are invariant to intramolecular mutual exchange are now near to the center of the spectrum due to the different signs and magnitudes of the coupling constants. Again the separation between these transitions is equal to the sum of the H–P coupling constants (*e.g.*, $J_{51} + J_{52} + J_{53} + J_{54}$). Hydride region shift data and the sum of the H–P coupling constants for some ruthenium dihydrides are given in Table III. The hydride region ^1H nmr spectra are typically less symmetric at 60, 90, and 100 MHz.

The spectra of $H_2Ru[PC_6H_5(OCH_3)_2]_4$, $H_2Ru[PC_6H_5(OC_2H_5)_2]_4$, and $H_2Ru\{PC_6H_5[OCH(CH_3)_2]_2\}_4$ can be interpreted in terms of a mixture of cis and trans isomers with about 15, 7.5 (Figure 10), and 7.5%, respectively. of the trans isomer in toluene-d_8 at room temperature.

The cis structure has been confirmed for four of the

(18) K. C. Dewhirst, W. Keim, and C. A. Reilly, *Inorg. Chem.*, 7, 546 (1968).

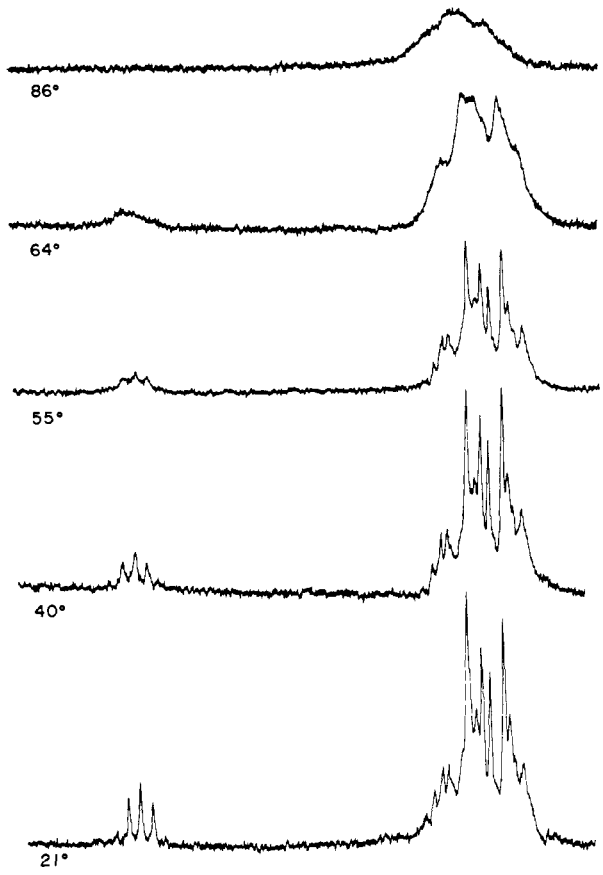

Figure 10. The temperature-dependent 220-MHz hydride region ^1H nmr spectrum for $H_2Ru[PC_6H_5(OC_2H_5)_2]_4$. The low-field end of the spectrum is at the left side.

line shapes are shown in Figure 11. The spectrum for $H_2Ru[P(OCH_3)_3]_4$ is almost identical with that shown for $H_2Ru[P(OC_2H_5)_3]_4$. The ^{31}P nmr parameters obtained from these spectra are given in Table IV.

Table IV. ^{31}P Nmr Parameters for Some Ruthenium Dihydrides at Room Temperature in Toluene Taken from the A_2B_2 Proton Noise Decoupled ^{31}P Spectra

Compound	J^a	δ^b	Shift^c
$H_2Ru[P(CH_3)_2C_6H_5]_4$	23	7.4	−11.0
$H_2Ru[P(C_6H_5)_2CH_3]$	18.5	10.39	−28.8
$H_2Ru[P(OC_2H_5)_3]_4$	41	3.29	−167.2
$H_2Ru[P(OCH_3)_3]_4$	41	3.40	−171.9

$^a J_{13} = J_{14} = J_{23} = J_{24}$ coupling constants in Hz. ^{b} Chemical shift differences for the two ^{31}P environments (ppm). ^{c} Ppm upfield from 85% H_3PO_4.

C. Stereochemical Nonrigidity and the Cis–Trans Equilibrium

The temperature dependence of the nmr spectra of the six-coordinate iron and ruthenium dihydrides can, for convenience, be divided into two classes. Class A consists of those complexes which have exclusively a cis structure and for which no evidence of a trans isomer can be obtained from the nmr spectra. Class B consists of those dihydrides for which both cis and trans isomers can either be observed separately in the low-temperature limit or are both required in order to interpret the nmr spectra at higher temperatures. As yet, we have found no examples of the possible third class consisting of exclusively trans molecules.

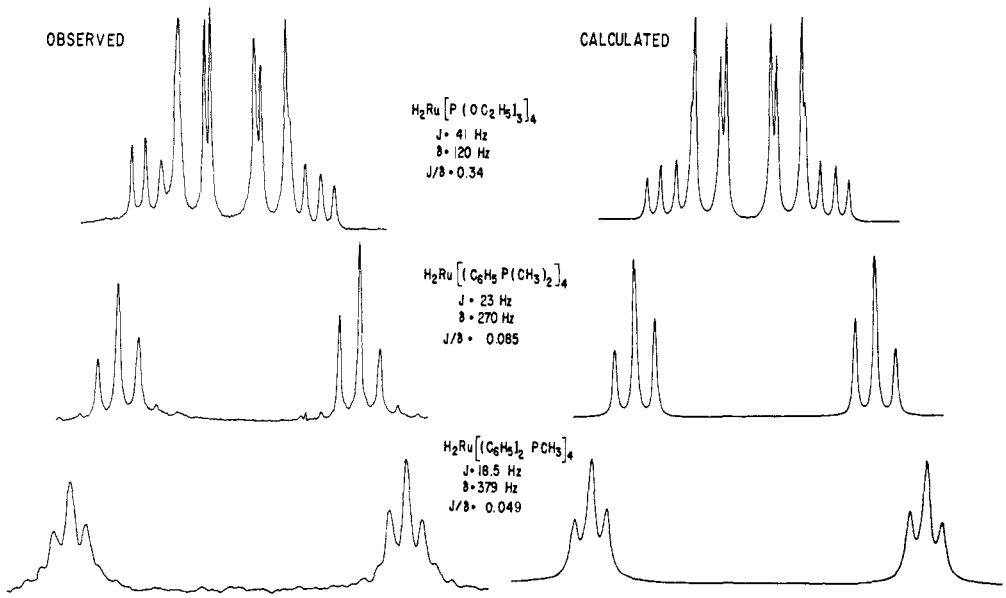

Figure 11. Low-temperature limit (room temperature) proton noise decoupled ^{31}P spectra taken at 36.43 MHz for three *cis*-ruthenium dihydrides. The calculated spectra assume an A_2B_2 ^{31}P spin system.

ruthenium dihydrides by the observation of A_2B_2 patterns for the proton noise decoupled ^{31}P spectra at room temperature. The observed ^1H noise decoupled ^{31}P spectra for three of these dihydrides together with computer simulated spectra based on an A_2B_2 high-resolution nmr Hamiltonian and Lorentzian (The "trans"[17] molecule, $H_2Fe\{o\text{-}C_6H_4[P(C_2H_5)_2]_2\}_2$ is discussed below.)

(1) Iron Dihydrides—Class A. Cis Molecules. Typical temperature-dependent hydride ^1H nmr spectra for a cis dihydride are shown in Figure 1. Other spectral illustrations may be found in ref 3 and 7–9.

Since the fraction of trans isomers is very small at all temperatures in the range covered in these studies, the temperature-dependent hydride spectra can be interpreted in terms of the high-resolution nmr Hamiltonian of the cis isomer alone. For the purposes of the line shape calculations the exchange can be considered as a mutual intramolecular process involving only the relabeling of the nuclear spins.

As the temperature is raised from the low-temperature limit, the spectrum begins to broaden as the exchange rate increases (with the exception of the sharp outer lines which correspond to transitions of the type $|H(\alpha\alpha);\ P(\alpha\alpha\alpha\alpha)\rangle \rightarrow |H(\alpha\beta + \beta\alpha);\ P(\alpha\alpha\alpha\alpha)\rangle$ which are invariant to exchange of the spin labels). On further temperature increase, the spectra broaden extensively and eventually coalesce into a symmetric binomial quintet. Since the chemical shift difference for the hydride protons in the cis and trans isomers is quite large (Figure 3, Figure 2 of ref 8) only a very small fraction ($\sim$1%) of the trans isomer exchanging with the cis isomer would be required to broaden the sharp outer lines. In those cases where there is a significant fraction of both isomers (see class B below), the averaging of the chemical shifts between the cis and trans environments completely dominates the nmr line shapes and no detailed mechanistic information can be obtained from them. The line shapes for the class A systems contain mechanistic as well as rate information, and a detailed analysis of the temperature-dependent nmr spectra for $H_2Fe[P(OC_2H_5)_3]_4$ has been described.[9] Figure 1 of ref 9 shows the observed and calculated 220-MHz ^1H hydride region nmr spectra of $H_2Fe[P(OC_2H_5)_3]_4$ at several temperatures. Since the appearance of the temperature-dependent hydride spectra of most of the iron dihydrides at 220 MHz is very similar to that for $H_2Fe[P(OC_2H_5)_3]_4$ and since the coupling constants are of very similar magnitude, the calculated spectra shown in Figure 1 of ref 9, and those at other temperatures (exchange rates) not shown, were used to obtain a good estimate of the rates of exchange of the other dihydrides by comparing the observed spectra with those calculated for $H_2Fe[P(OC_2H_5)_3]_4$. The free energies of activation were then derived from the Eyring equation

$$R(T) = K(kT/h)e^{-\Delta G^{\ddagger}/RT} \qquad (1)$$

assuming the transmission coefficient, K, to be equal to 1. Where the low-temperature-limit spectra deviated significantly from that of $H_2Fe[P(OC_2H_5)_3]_4$ ($H_2Fe[P(OCH_2)_3CC_2H_5]_4$, for example; see Figure 1), a separate first-order density matrix line shape analysis was carried out. The activation parameters are listed in Table V for some cis iron dihydrides. Because the slow-exchange-limit ^1H nmr spectrum for $H_2Fe(PF_3)_4$ was not analyzed in detail and because the spectrum is very different from those of the other dihydrides due to the quite large HF couplings, the value for this molecule in Table V is only an estimate ($\sim \pm 1$ kcal mol^{-1}).

(2) Iron Dihydrides—Class B. Cis and Trans Molecules. $H_2Fe[PC_6H_5(OC_2H_5)_2]_4$ and $H_2Fe[PC_6H_5(OCH_3)_2]_4$ show significant concentrations of both cis and trans isomers in solution. The temperature-dependent hydride ^1H nmr spectra for these molecules are quite different from those observed for the hydrides of class A. A typical example is shown in Figure 3, together with spectra simulated assuming a random exchange mechanism and a first-order approximation.

Table V. Free Energies of Activation for Exchange in Some Iron Dihydrides

Compound	Temp, °C	Rate, sec^{-1}	$\Delta G^{\ddagger}$ [a]
$H_2Fe\{o\text{-}C_6H_4[P(C_2H_5)_2]_2\}_2$			11.5[b,d]
$H_2Fe[PC_6H_5(OC_2H_5)_2]_4$	−19	150	12.2[c,d]
$H_2Fe[PC_6H_5(OCH_3)_2]_4$	−5	500	12.3[c,d]
$H_2Fe[PCH_3(C_6H_5)_2]_4$	−5	275	12.6
$H_2Fe[P(O\text{-}i\text{-}C_3H_7)_3]_4$	21	450	13.6
$H_2Fe[P(OC_2H_5)_3]_4$			13.7[c]
$H_2Fe[P(O\text{-}i\text{-}C_3H_7)_2C_6H_5]_4$	24	400	13.8
$H_2Fe[P(CH_3)_2C_6H_5]_4$	22	300	13.9
$H_2Fe[PF_3]_4$	67	~5000	~14.0[b]
$H_2Fe[P(C_2H_5)_2C_6H_5]_4$	22	200	14.1
$H_2Fe[(C_6H_5)_2PCH_2CH_2P(C_6H_5)_2]_2$	22	150	14.3
$H_2Fe[P(OCH_2)_3CC_2H_5]_4$	55	720	14.9[c]
$H_2Fe[P(OC_6H_5)_3]_4$	66	1000	15.2
$H_2Fe[P(O\text{-}o\text{-}tolyl)_3]_4$	60	200	16.0
$H_2Fe[(CH_3)_2PCH_2CH_2P(CH_3)_2]_2$	79	600	16.2
$H_2Fe[P(C_6H_5)_2C_2H_5]_3CO$	22	3000	12.5
$H_2Fe[P(C_6H_5)_2CH_3]_3CO$	10	1200	12.5

[a] Free energy of activation, kcal mol^{-1}. [b] Crude estimate. [c] These spectra were simulated individually. [d] Cis → trans.

The deviation of the intensities in the trans isomer from a binomial quintet at low temperatures for $H_2Fe[PC_6H_5(OCH_3)_2]_4$ is quite evident on comparing the observed spectrum at −38° with the calculated slow-exchange-limit spectra. The spectra in Figure 3 are simulated assuming that the chemical shift difference between the cis and trans hydride protons is temperature independent. As the temperature is raised from the low-temperature limit the fraction of cis isomer increases and the spectra begin to broaden. Because of the averaging of the cis and trans sites there are no sharp lines at intermediate exchange rates. As the temperature is raised still further, the proportion of cis isomer continues to increase and eventually the spectrum sharpens into a symmetric binomial quintet. The chemical shift of the averaged quintet indicates that at the high-temperature limit the equilibrium favors the cis isomer (~15% trans, 85% cis at 83° for $H_2Fe[PC_6H_5(OCH_3)_2]_4$ in toluene-d_8, see Figure 3). The analysis of the temperature-dependent spectra of $H_2Fe[PC_6H_5(OCH_3)_2]_4$ yields both rate and equilibrium data but no additional mechanistic data. For the equilibrium K_{eq} = [cis]/[trans], $\Delta H \cong 3$ kcal mol^{-1} and $\Delta S \cong 11$ cal mol^{-1} deg^{-1} showing, as is clear from Figure 3, that the enthalpy factor favors the trans isomer and the entropy factor favors the cis isomer. The temperature-dependent hydride ^1H spectra of $H_2Fe[PC_6H_5(OC_2H_5)_2]_4$ are very similar (Figure 2 of ref 8) except that the fraction of trans isomer is somewhat smaller. The next member in the series, $H_2Fe\{PC_6H_5[OCH(CH_3)_2]_2\}_4$, appears to be totally cis (Figure 1 of ref 8). We have no explanation at this time for the dependence of the cis/trans equilibrium constant on these small changes in the ligand.

The free energies of activation for the cis → trans step are given in Table V. It is significant that the cis → trans exchange rates are comparable to the rates of mutual exchange in the class A molecules.

(3) Compound 1. The slow-exchange limit, hydride ^1H spectra (Figure 7), and noise decoupled ^{31}P spectra (Figure 8) indicate that this molecule is almost

exclusively trans in the low-temperature limit. (A search was made for evidence of the cis isomer in both the proton and ^1H noise decoupled ^{31}P spectra but none was found.) As the temperature is raised, the hydride region proton spectrum at first broadens and then coalesces to a new binomial quintet which is considerably to the high-field side of the original quintet (Figure 7). We interpret these spectra in terms of an exchange of the trans with the cis isomer whose population increases as the temperature is raised. This is supported by the observation that the trans isomer itself cannot give rise to the observed line shape effects and that the shift to higher field as the temperature is raised is consistent with the fact that the cis hydride resonance is appreciably to the high-field side of the trans resonance in those cases where both cis and trans resonances can be observed in the low-temperature limit. Similarly, the temperature dependence of the noise decoupled ^{31}P spectra which broadens from a sharp singlet and then sharpens again as the temperature is raised (Figure 8), accompanied by a strong temperature dependence of the average chemical shift, can best be explained in terms of nonmutual intramolecular exchange between at least two sites.

(4) Solvent Dependence of Cis–Trans Equilibrium. Whereas the rate of exchange of $H_2Fe[P(OC_2H_5)_3]_4$ has been found to be almost independent of the solvent,[9] the cis–trans equilibrium constants for $H_2Fe[PC_6H_5(OCH_3)_2]_4$ and for $H_2Fe[PC_6H_5(OC_2H_5)_2]_4$ are found to be quite strongly dependent on the solvent. The equilibrium constant value in a variety of solvents at $-50°$ are given in Table VI. As might be

Table VI. Equilibrium Constants for $H_2Fe[P(OC_2H_5)_2C_6H_5]_4$ in Some Solvents

Solvent	Dielectric (20°)	K_{eq} (cis/trans)
n-Hexane	1.9	0.95
Toluene	2.4	1.96
Diethyl ether	4.4	1.15
Chloroform	4.8	7.00
Chlorobenzene	5.7	3.31
Methylene chloride	9.1	6.52

expected, the more polar cis isomer is favored by the solvents with the larger dielectric constants. However, there is no smooth correlation between the equilibrium constant and dielectric constant; specific solvent interactions, such as hydrogen bonding, are probably operative for solvents like dichloromethane and chloroform.

(5) Ruthenium Dihydrides. The barriers to intramolecular rearrangement in the ruthenium dihydrides (Figures 9, 10, 12 and Table VII) are larger than those observed for the iron dihydrides. The fast-exchange-limit ^1H spectra of the ruthenium dihydrides should be binomial quintets as in the iron dihydrides. Unfortunately, we have not yet observed a high-temperature-limiting spectrum. In the case of the ruthenium dihydrides, the sharp lines which are invariant to the exchange process and which would become the outer lines of the high-temperature quintet are quite close together (Figures 9 and 12), *i.e.*, the averaged H–P coupling constant is small. Consequently, the exchange rate must be quite fast for the quintet to be resolvable. This requirement combined with that of a larger barrier to exchange for the ruthenium hydrides demands such a high temperature for collapse that other processes (ligand dissociation and decomposition) begin to dominate before the high-temperature limit is reached.

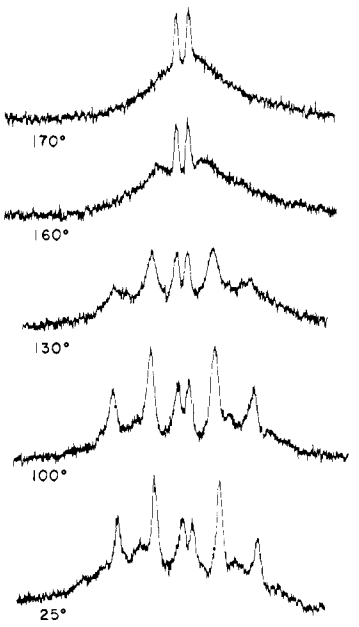

Figure 12. The 100-MHz hydride region ^1H nmr spectrum of $H_2Ru[PC_6H_5(CH_3)_2]_4$ taken at several temperatures.

Table VII. Free Energies of Activation for Exchange in Some Ruthenium Dihydrides

Compound	Temp, °C	Rate, sec^{-1}	$\Delta G^{\ddagger}$ [a]
$H_2Ru[P(C_6H_5)_2OCH_3]_4$	80	400	16.5
$H_2Ru[PC_6H_5(OC_2H_5)_2]_4$	65	50	17.2[b]
$H_2Ru[PC_6H_5(OCH_3)_2]_4$	77	50	17.8[b]
$H_2Ru[P(C_6H_5)_2CH_3]_4$	120	300	18.7
$H_2Ru[PC_6H_5(C_2H_5)_2]_4$	102	75	19.1
$H_2Ru[C_6H_5PCH_2CH_2PC_6H_5]_2$	140	500	19.3
$H_2Ru[P(OCH_3)_3]_4$	100	20	19.7
$H_2Ru[PC_6H_5(CH_3)_2]_4$	130	100	20.1
$H_2Ru[PF_3]_4$	90	$\leqslant 25$	$\geqslant 19.0$
$H_2Ru\{P[OCH(CH_3)_2]_3\}_4$	100	$\leqslant 25$	$\geqslant 19.5$
$H_2Ru[P(OC_2H_5)_3]_4$	110	$\leqslant 50$	$\geqslant 19.0$

[a] Free energy of activation, kcal mol^{-1}. [b] Cis → trans barrier.

Figure 13 shows the nmr line shapes as a function of exchange rate for the four permutational mechanisms I–IV discussed in ref 9.[19,20] In contrast to the

(19) The slow exchange limit nmr parameters used in these simulations are those used to simulate the room temperature ^1H nmr spectrum of $H_2Ru[P(OCH_3)_3]_4$ in toluene-*d*, shown in Figure 9.

(20) For the convenience of the reader, we restate the basic permutational sets for the *cis*-H_2MP_4 system of C_{2v} symmetry using the numbering scheme in Figure 2.

	Basic set	Equivalent sets		
E	(12) (34) (56)	(1) (2) (3) (4) (5) (6)	(34) (56)	(12)
I	(14) (23) (56)	(13) (24)	(1324) (56)	(1423)
	(13) (24) (56)	(14) (23)	(1423) (56)	(1324)
II	(12) (34)	(56)	(34)	(12) (58)
III	(14) (56)	(1243)	(124) (56)	(143)
	(23) (56)	(1342)	(132) (56)	(234)
	(24) (56)	(1432)	(142) (56)	(243)
	(13) (56)	(1234)	(123) (56)	(134)
IV	(14)	(1243) (56)	(124)	(143 (56)
	(23)	(1342) (56)	(132)	(234) (56)
	(24)	(1432) (56)	(142)	(243) (56)
	(13)	(1234) (56)	(123)	(134) (56)

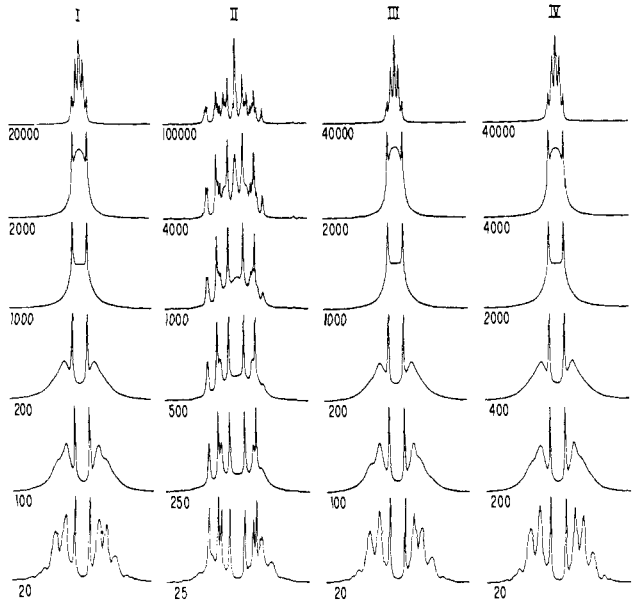

Figure 13. Calculated nmr line shapes as a function of exchange rate for the basic permutational mechanisms I–IV discussed in ref 9. These simulations are intended to correspond to the hydride region ^1H nmr spectra of $H_2Ru[P(OCH_3)_3]_4$ taken at 90 MHz. The exchange rates are in units of sec^{-1}. The slow-exchange-limit spectra (identical in all cases) have been omitted from this figure and are all identical with that shown at the bottom of Figure 9.

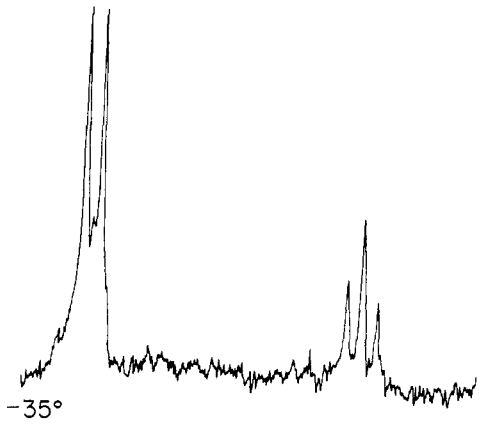

Figure 14. The proton noise decoupled ^{31}P (36.43 MHz) nmr spectrum of $H_2FeCO[P(C_6H_5)_2C_2H_5]_3$ in toluene at −35°.

case of $H_2Fe[P(OC_2H_5)_3]_4$ (ref 9) where all four permutational sets gave quite distinct nmr line shapes over a wide range of exchange rates, the sets I, III, and IV in the present case give rise to almost indistinguishable line shapes at all rates of exchange except for those near the slow-exchange limit. A much better fit to the slow-exchange-limit spectrum than that shown in Figure 9 (after some 500 trial and error simulations of the low-temperature-limit spectrum) is required for meaningful mechanistic information to be obtained from the spectra. The permutational mechanism II which gives a different high-temperature-limit spectrum is, of course, readily distinguishable from the other three. The indistinguishability of permutational mechanisms I, III, and IV in this case can be attributed to the fact that the high-temperature-limit averaged H–P coupling constant is small and all the lines in the

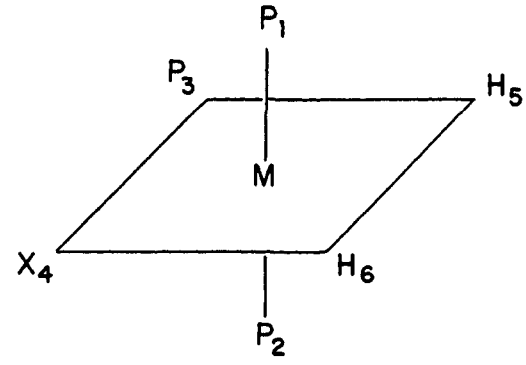

Figure 15. Nuclear labeling scheme and idealized octahedral geometry for the *cis*-H_2ML_3X systems. Departure from this idealized geometry similar to that shown in Figure 2 is anticipated.

spectrum are averaged almost to the same frequency. Consequently, the temperature-dependent ruthenium hydride spectra contain less rate and mechanistic data than do the iron dihydrides, and a detailed analysis has not as yet been carried out for any of them. The free energies of activation can, however, be estimated fairly reliably by comparing the observed spectra with simulations such as that shown in Figure 13 to obtain a crude estimate of the exchange rate at some chosen temperature. Activation parameters can then be estimated using the Eyring equation. Data estimated in this manner using the simulation spectra obtained from mechanism IV are shown in Table VII. (The choice of permutation set IV is arbitrary; sets I, III, or IV or combinations thereof would yield essentially the same simulations.)

The hydride region ^1H spectra of $H_2Ru[PC_6H_5(OCH_3)_2]_4$, $H_2Ru[PC_6H_5(OC_2H_5)_2]_4$ (Figure 11), and $H_2Ru\{PC_6H_5[OCH(CH_3)_2]_2\}_4$ have some similarities with the spectra of the iron dihydrides where both cis and trans isomers are observed.

(a) The hydride resonance of the trans isomer is to low field of that for the cis isomer.

(b) There are no lines which remain sharp through the whole exchange region.

(c) The exchange rate is faster than for most of the exclusively cis-dihydrides.

The H–P coupling constant for the trans isomer is now small (21 Hz in all three complexes) in accordance with the small cis coupling constants observed in the cis isomer. In the corresponding iron dihydrides where large cis coupling constants are found in the cis isomer the coupling constant for the trans isomer is also large (47.5 Hz for $H_2Fe[PC_6H_5(OC_2H_5)_2]_4$).

(6) Molecules of the Type H_2ML_3X (M = Fe, Ru). The low-temperature-limit ^1H noise decoupled ^{31}P nmr spectrum of $H_2Fe(CO)[P(C_6H_5)_2C_2H_5]_3$ is an AB_2 pattern (Figure 14). This spectrum is consistent with the cis dihydride structure shown in Figure 15 in which there is one unique and two equivalent ^{31}P nuclei. The last row of Figure 16 shows the 220-MHz hydride region ^1H nmr spectrum at −32° together with a calculated spectrum based on the structure shown in Figure 15. Nmr parameters used to obtain the simulated spectra are given in Table VIII.

An exchange process occurs for $H_2Fe(CO)[P(C_6H_5)_2C_2H_5]_3$ and $H_2Fe(CO)[P(C_6H_5)_2CH_3]_3$ as shown by the temperature dependence of the hydride resonances

Table VIII. Nmr Parameters for $H_2Fe(CO)[P(C_6H_5)_2C_2H_5]_3$[a]

J_{12}	unknown (magnetic equivalence)
$\|J_{13}\| = \|J_{23}\|$	18 Hz
$J_{15} = J_{25}$	± 54 Hz
$J_{16} = J_{26}$	± 72 Hz
J_{35}	± 54 Hz
J_{36}	± 17 Hz
$\|J_{56}\|$	17 Hz
$\delta_1 = \delta_2$	-73.0 ppm[b]
δ_3	-64.2 ppm[b]
δ_5	$+11.7$ ppm[c]
δ_6	$+9.0$ ppm[c]

[a] The nuclear labeling scheme is shown in Figure 15. The assignment of the protons H_5 and H_6 is not unambiguous on the basis of the nmr spectra alone. The present assignment is obtained assuming that the "cis" coupling constants J_{15}, J_{25}, J_{35} are of comparable magnitude and the trans coupling constant J_{36} is small. [b] Upfield from 85% H_3PO_4. [c] Upfield from TMS.

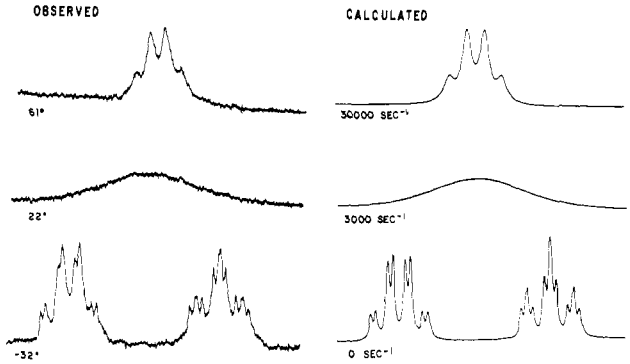

Figure 16. The temperature-dependent 220-MHz hydride region ^1H nmr spectrum of $H_2Fe[P(C_6H_5)_2C_2H_5]_3CO$. The low-field end of the spectrum is at the left side. The calculated spectra in this figure are for a random exchange permutational mechanism.

(Figure 16). As the temperature is raised, the spectra at first broaden and then sharpen to a quartet, indicating that both the ^1H and ^{31}P environments have become averaged on the nmr time scale. Because this involves the averaging of the two hydride chemical shifts there are no sharp lines invariant to the exchange process despite the fact that the exchange is probably mutual. Maintenance of H–P coupling in the high-temperature limit demonstrates that the rearrangement does not involve dissociation of either the hydride or phosphine ligands. We have no similar, direct evidence that dissociation of the CO ligand is not involved but consider rapid CO dissociation to be unlikely.

Since the line shapes are dominated by the averaging of the chemical shifts, they are sensitive to the exchange mechanism only near the slow-exchange limit where the differences for different mechanisms may be quite subtle. There is, however, some mechanistic information in the fast-exchange-limit spectra (see Appendix I). In Figure 16 the observed temperature-dependent ^1H nmr spectra for $H_2Fe(CO)[P(C_6H_5)_2C_2H_5]_3$ are compared with spectra simulated assuming a random exchange permutational mechanism (Appendix I). The exchange rates (exchange barriers) for $H_2Fe[P(C_6H_5)_2CH_3]_4$ and $H_2Fe(CO)[P(C_6H_5)_2C_2H_5]_3$ are remarkably similar: 12.6 and 12.5 kcal/mol^{-1}, respectively (Table V).

The hydride resonance of $H_2Ru[P(C_6H_5)_3]_3C_6H_5CN$ begins to broaden at about 60°, corresponding to an activation energy of about 17 kcal/mol^{-1}. The process responsible for these line shape effects is probably dissociation of benzonitrile; this ligand, unlike the phosphine or carbon monoxide ligands, is rapidly dsplaced by strong π-bonding ligands.

D. Discussion of Exchange Mechanisms

In the earlier detailed analysis[9] of the temperature-dependent nmr line shapes for $H_2Fe[P(OC_2H_5)_3]_4$ it was shown that for the hydride ^1H spectra there are five basic types of temperature dependence for the nmr line shapes, including essentially temperature-independent spectra (the basic permutational sets I, II, III, IV, and E in ref 9).[20] Only the basic permutational set IV and linear combinations of the basic sets containing a large fraction of permutations belonging to IV gave calculated spectra in good agreement with the observed spectra. On the basis of these results and the X-ray structural data for *cis*-$H_2Fe[C_6H_5P(OC_2H_5)_3]_4$, we proposed two possible physical mechanisms for the exchange process.

Mechanism A consists of a shift of a hydride nucleus from an unoccupied to a vacant face of a nearly regular tetrahedral arrangement of phosphorus atoms by traverse of a tetrahedral edge. This exchange process corresponds to the basic permutational mechanism IV which gives excellent agreement between the observed and calculated temperature-dependent line shapes.[9] We gave this mechanism the possibly misleading descriptive title "tetrahedral tunneling," but as we noted originally this does not imply a quantum mechanical tunneling of the hydride hydrogens without motion of the other ligands. A better descriptive title is the "tetrahedral jump" model. The structural parameters for the cis isomer demand a considerable motion of the phosphorus ligands for the observed mutual exchange process. A comparison of the temperature-dependent ^1H nmr spectra assigned to the CH_2 protons for $H_2Fe[P(OC_2H_5)_3]_4$ and $D_2Fe[P(OC_2H_5)_3]_4$ (Figure 17) indicates that the isotope effect on deuteration is quite small and implies that the motion of the phosphorus ligands makes the major contribution to the reduced mass for the exchange process. A considerable opening of the P_nFeP_m bond angle would be expected as the hydride approaches the P_nP_m edge in the transition state.

Mechanism B consists of simultaneous motion of the hydride hydrogens from face positions to trans edge positions corresponding to the distorted D_{2d} trans structure shown in Figure 4, with the trans intermediate sufficiently long lived such that the hydrogens move with equal probability back to previously occupied faces or on to previously unoccupied faces and that the inversion shown in Figure 4 does not on average occur while the molecule is near the trans configuration. This physical mechanism corresponds to the linear combination of basic permutational sets $2E + I + IV$. (Since E contains only one permutation and has no effect, I contains two permutations and IV contains four permutations, this permutational mechanism is predominantly IV.) For this mechanism, the agreement between calculated and observed spectra is not as good for IV alone but is acceptable. Figure 18 compares the observed 90-MHz hydride nmr spectra for $H_2Fe[P(OC_2H_5)_3]_4$ with spectra calculated for the permutational mechanism $2E + I + IV$. This figure should be compared with Figure 2 of ref 9 where the results for the basic set IV alone

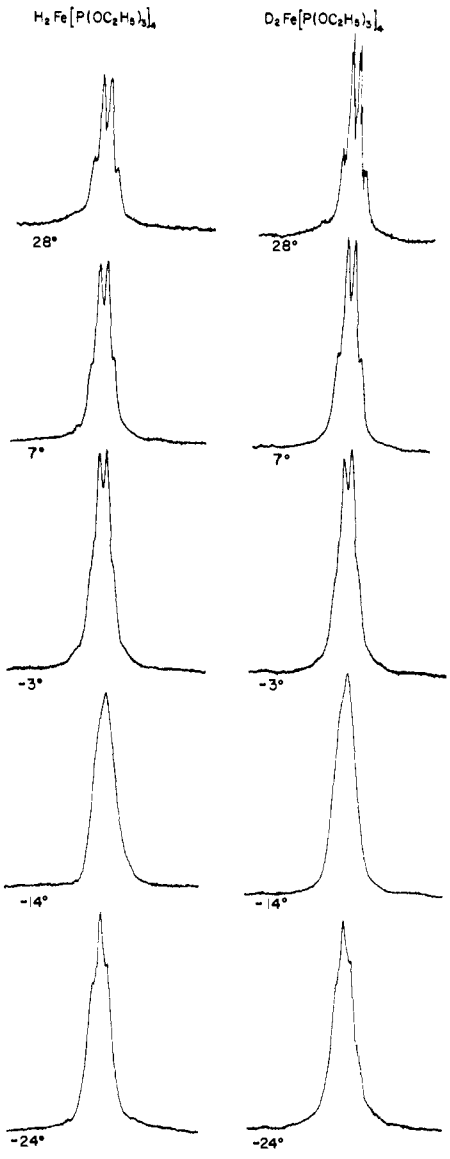

Figure 17. A comparison of the temperature-dependent 90-MHz ^1H nmr spectra assigned to the CH_2 protons of $H_2Fe[P(OC_2H_5)_3]_4$ and $D_2Fe[P(OC_2H_5)_3]_4$.

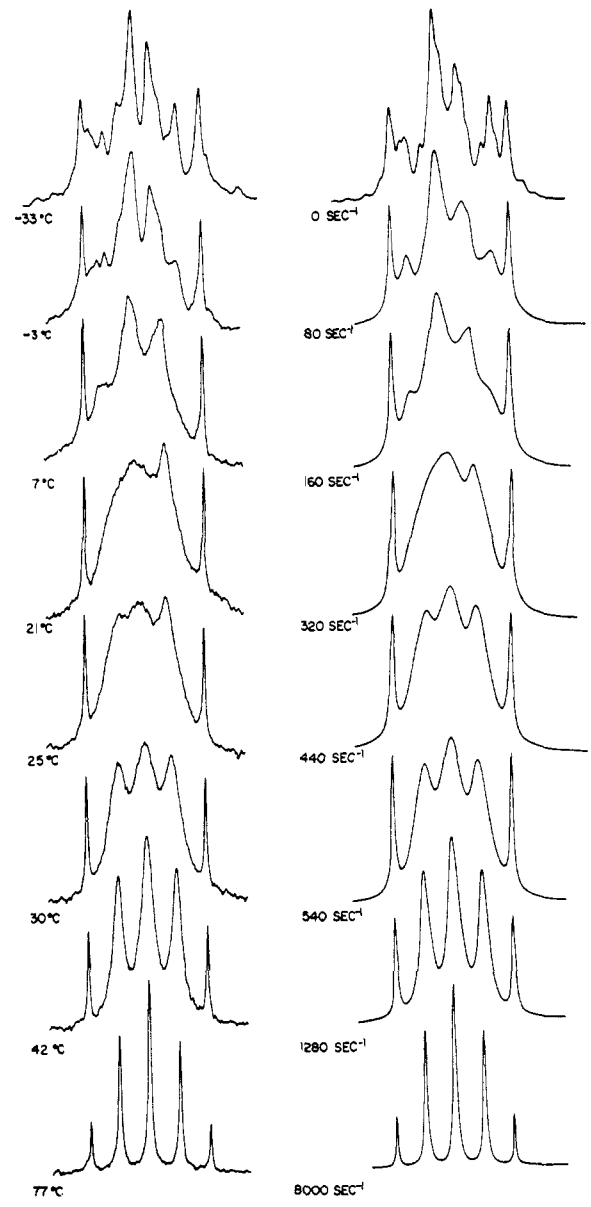

Figure 18. Observed and calculated 90-MHz ^1H nmr spectra for $H_2Fe[P(OC_2H_5)_3]_4$. The calculated spectra are for the permutational mechanism[9] $2E + I + IV$.

are shown. The agreement is somewhat better in the earlier case, but uncertainties due to the imperfect fit to the low-temperature-limit spectra and unknown temperature dependence of coupling constants make a sharp distinction between mechanisms A and B difficult on this basis.

Mechanism B is attractive since it does involve the trans isomer. It is significant that in those cases where both cis and trans isomers can be observed the cis → trans exchange rate is faster than the cis → cis (cis → trans → cis) exchange in the complexes which are exclusively cis. Further circumstantial evidence for mechanism B comes from the observation that in the low-temperature limit the hydride resonance of *trans*-$H_2Fe[PC_6H_5(OCH_3)_2]_4$ and *trans*-$H_2Fe[PC_6H_5(OC_2H_5)_2]_4$ are nonbinomial quintets. These data are consistent with an D_{2d} structure (Figure 4) in which the inversion process is slow on the nmr time scale at these temperatures. suggesting that the barrier to inversion may be substantial. We have no structural parameters for a *trans*-iron dihydride molecule, but we have such parameters from an X-ray study of *trans*-$H_2Ru[PC_6H_5(OC_2H_5)_2]_4$.[14] This molecule has the D_{2d} structure, but the displacement from D_{4h} is rather small.[14b]

The permutational mechanism $2E + 2I + 2II + III + IV$ corresponding to a *trans intermediate* with inversion of the phosphorus framework gives calculated line shapes in poor agreement with experiment. Similarly, if the mechanism is concerted with a *trans transition state* rather than a *trans intermediate* and the hydrogens always move simultaneously from occupied to previously unoccupied faces, the permutational mechanism is I and again the spectra simulated for this mechanism are in poor agreement with the observed spectra. For systems of the type $H_2M(L_2)_2$, the observation of a high-temperature quintet requires rapid inversion of the trans isomer. In this case one would expect ring strain in the distorted trans intermediate to reduce the barrier to inversion.

It is probable that we are dealing with a continuum of reaction coordinates similar to those shown in Figure 19.

Table IX

Subclass	Basic permutational set	Equivalent basic permutational set
E	$\begin{pmatrix}1&2&3&5&6\\1&2&3&5&6\end{pmatrix} = E$	$\begin{pmatrix}1&2&3&5&6\\2&1&3&5&6\end{pmatrix} = (12)$
α	$\begin{pmatrix}1&2&3&5&6\\3&2&1&6&5\\1&3&2&6&5\end{pmatrix} = \begin{matrix}(13)(56)\\(23)(56)\end{matrix}$	$\begin{pmatrix}1&2&3&5&6\\2&3&1&6&5\\3&1&2&6&5\end{pmatrix} = \begin{matrix}(123)(56)\\(132)(56)\end{matrix}$
β	$\begin{pmatrix}1&2&3&5&6\\3&2&1&5&6\\1&3&2&5&6\end{pmatrix} = \begin{matrix}(13)\\(23)\end{matrix}$	$\begin{pmatrix}1&2&3&5&6\\2&3&1&5&6\\3&1&2&5&6\end{pmatrix} = \begin{matrix}(123)\\(132)\end{matrix}$
γ	$\begin{pmatrix}1&2&3&5&6\\2&1&3&6&5\end{pmatrix} = (12)(56)$	$\begin{pmatrix}1&2&3&5&6\\1&2&3&6&5\end{pmatrix} = (56)$

Curve (a) corresponds to the case where there is no intermediate in the cis mutual exchange process. The transition state would then have to correspond to the one suggested for the connected "tetrahedral jump" process. Curve (b) corresponds to the case of a short-lived *intermediate* (the trans structure without inversion), and curve (c) corresponds to the situation where there are appreciable quantities of cis and trans molecules in equilibrium. It would not be unreasonable to suppose that the barriers in cases of type (c) should be lower than those for cases nearer to (a) or (b) because of the increase in the effective order of the potential function.

Despite the fact that the ligands in these hydrides varied widely in electronic and steric character, the range of observed barriers is quite small (Tables V and VII). There appears to be no correlation between the magnitude of these barriers and the ligand cone angle[21] or the ligand electronic character. All iron complexes probably have similar structural parameters in cis and trans stereochemistry. The ruthenium barriers are substantially larger than the iron barriers. We originally suggested that this reflected a closer approximation of an octahedral geometry for the ruthenium complexes since the P–P repulsions would be less significant with this larger central nucleus. We are searching for an X-ray test of this thesis through a comparison of *trans*-$FeH_2[PC_6H_5(OC_2H_5)_2]_4$ with *trans*-$RuH_2[PC_6H_5(OC_2H_5)_2]_4$.[14b] This would provide a further intercomparison with *cis*-$FeH_2[PC_6H_5(OC_2H_5)_2]_4$.[14a] However, it does not necessarily follow that the rearrangement mechanism for the ruthenium complexes is similar to that for the iron complexes, and the nmr data for the former have not provided to date the relatively incisive identification of the permutational mechanism as was effected for the latter complexes. Finally it may be noted that the commonly accepted stereochemical rule that trans P–H couplings in transition metal hydrides are much larger than the corresponding cis couplings breaks down for the iron dihydrides, although it still holds for the ruthenium complexes. Breakdown of this stereochemical rule could, as we have discussed before, reflect the quite severe departure from the octahedral 180°, 90° angles in iron complexes.

Acknowledgments. We would like to thank Dr. D. H. Gerlach, Mr. W. G. Peet, and Mr. M. A. Cushing for preparation of the complexes, and Mr. G. Watunya and Mr. F. W. Barney for obtaining some of the nmr spectra.

(21) C. A. Tolman, *J. Amer. Chem. Soc.*, **92**, 2956 (1970).

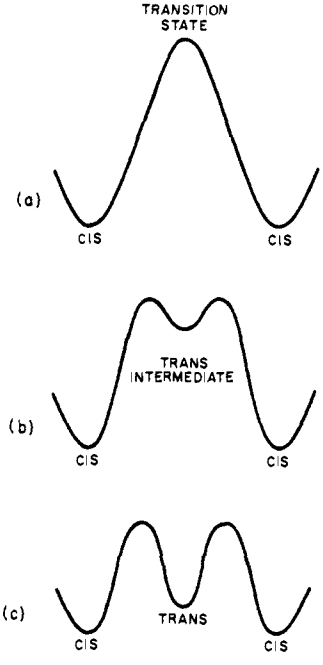

Figure 19. Schematic reaction coordinates: case (a), single hydrogen motion transition state; case (b), trans intermediate without inversion; case (c), cis and trans molecules in equilibrium.

Appendix I

Permutation Mechanistic Considerations[9] for Systems of the Type H_2ML_3X. Molecules of this type with the cis structure shown in Figure 15 belong to the point group C_s with the two elements E and σ. There are $3! \times 2! = 12$ possible permutations which convert a labeled molecule into all possible labeled molecules with the same configuration, *i.e.*, the product of all permutations of the phosphorus atoms among themselves and all possible permutations of hydrogens among themselves.

Using the numbering in Figure 15, the operators of the point group C_s can be written

$$E\begin{pmatrix}1&2&3&5&6\\1&2&3&5&6\end{pmatrix} = (1)(2)(3)(5)(6)$$

$$\sigma\begin{pmatrix}1&2&3&5&6\\2&1&3&5&6\end{pmatrix} = (12)(3)(5)(6)$$

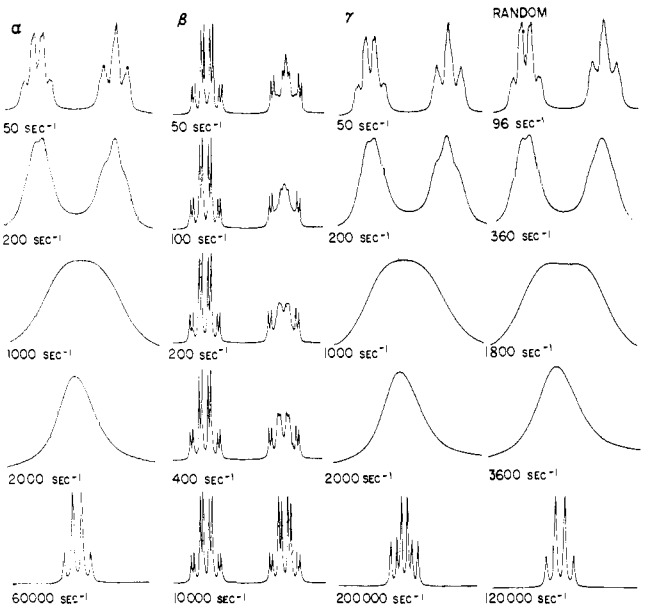

Figure 20. Calculated ^1H nmr line shapes for an H_2ML_3X system for the permutational mechanisms α, β, γ, and $(E + \alpha + \beta + \gamma)$ at several exchange rates. The calculated slow-exchange-limit spectra (identical in all cases) have been omitted from this figure and are the same as that shown at the bottom of Figure 16.

in terms of the five nuclei of spin $^1/_2$ which are involved in the nmr Hamiltonian (X is considered to have zero spin). The Hamiltonian is invariant to the permutations E and σ. Thus, there are $12/2 = 6$ unique high-resolution nmr Hamiltonians for the five-spin system. Decomposition of the group into double cosets with respect to the elements of C_s indicates that there are a total of four permutational subclasses[9] (Table IX). Only α of these permutational subclasses give the correct high-temperature-limiting quartet. Mechanism β averages the H–P coupling constants but does not average the hydride chemicals shifts so that the high-temperature limit consists of two, not quite first order, doublets of quartets. Mechanism γ averages the hydride chemical shifts but does not average the H–P coupling constants and the high-temperature limit is a doublet of triplets. Thus any mechanism corresponding to β alone or γ alone can be ruled out. Mechanism α gives the correct high-temperature limit since both the H–P coupling constants and hydride shifts are averaged; similarly, any linear combination of α, β, and γ will give the correct high-temperature limit. One such linear combination is the random exchange mechanism. By random exchange we mean all permutations in the E, α, β, and γ subclasses equally weighed. In Figure 20, the results of a complete density matrix simulation of the nmr line shapes expected from the permutational mechanisms α, β, γ and random exchange. The nmr parameters used in this calculation are quite similar to those given in Table VIII.

Germanium-73 Nuclear Magnetic Resonance Spectra of Germanium Tetrahalides

R. G. Kidd* and H. G. Spinney

Contribution from the Department of Chemistry, University of Western Ontario, London 72, Ontario, Canada.
Received February 23, 1972

Abstract: The ^{73}Ge chemical shifts for $GeCl_4$, $GeBr_4$, GeI_4, and all 12 of the mixed tetrahalogermanes have been measured. The chemical shifts of these species are not a linear function of halogen coordination, but show a second-order dependence which can be rationalized using the pairwise additivity model. The shielding effect of the halogens increases in the order Cl < Br < I. The rate at which halogens redistribute between germaniums in liquid mixtures of the neat tetrahalogermanes is slow.

Of the elements from group IV of the periodic table, germanium alone has heretofore escaped the attention of the nmr spectroscopist motivated toward the establishment of molecular structure. Although carbon-13, reflecting its position at the center of things chemical, has received the most study, silicon-29, tin-119, and lead-209 have all produced spectra suitable for establishing the chemical shift ranges experienced by these nuclei.

We can now report that the pattern and range of chemical shifts displayed by germanium-73 are consistent with those exhibited by other group IV elements. The range in the case of the germanium tetrahalides spans 1117 ppm between $GeCl_4$ and GeI_4, which falls between the 1550 ppm range for the corresponding tin compounds and the 395 ppm range for the corresponding carbon compounds. In addition, the halogen-dependence pattern for the germanium shifts, with the tetraiodide signal occurring to high field of the tetrachloride signal, is the same as that observed for the tetrahalo compounds of the other main-group elements, such as ^{11}B,[1] ^{13}C,[2] ^{27}Al,[3] ^{29}Si,[4] ^{71}Ga,[5] ^{115}In,[6] and ^{119}Sn.[7]

The germanium tetrahalides constitute the best

(1) R. J. Thompson and J. C. Davies, *Inorg. Chem.*, **4**, 1464 (1965).
(2) W. M. Litchman and D. M. Grant, *J. Amer. Chem. Soc.*, **90**, 1400 (1968).
(3) R. G. Kidd and D. R. Truax, *ibid.*, **90**, 6867 (1968).
(4) B. K. Hunter and L. W. Reeves, *Can. J. Chem.*, **46**, 1399 (1968).
(5) J. W. Akitt, N. N. Greenwood, and A. Storr, *J. Chem. Soc.*, 4410 (1965).
(6) T. H. Cannon and R. E. Richards, *Trans. Faraday Soc.*, **62**, 1378 (1966).
(7) J. J. Burke and P. C. Lauterbur, *J. Amer. Chem. Soc.*, **83**, 326 (1961).